Inorganic Chemistry
Article

Inorg. Chem. **2010**, *49*, 5271–5275 **5271**
DOI: 10.1021/ic100378p

Metal-Dependent Phase Selection in Coordination Polymers Derived from a C_{2v}-Symmetric Tricarboxylate

Choong-Sun Lim, Jennifer K. Schnobrich, Antek G. Wong-Foy, and Adam J. Matzger*

Department of Chemistry and Macromolecular Science and Engineering Program, The University of Michigan, 930 North University Avenue, Ann Arbor, Michigan 48109-1055

Received February 24, 2010

Reacting biphenyl-3,4′,5-tricarboxylic acid (H_3BHTC) with the appropriate metal salt yields the microporous coordination polymers (MCPs) $Mn_3(BHTC)_2$ (**1**), $Mg_3(BHTC)_2$ (**2**), and $Co_3(BHTC)_2$ (**3**) containing hourglass metal clusters. The addition of Cu to reactions with Co^{II}, Fe^{III}, or Mn^{II} leads to the formation of heterobimetallic UMCM-150 isostructural analogues $Co_1Cu_2(BHTC)_2$ (**4**), $Fe_1Cu_2(BHTC)_2$ (**5**), and $Mn_1Cu_2(BHTC)_2$ (**6**) containing both paddlewheel and trinuclear metal clusters. X-ray diffraction analysis of the crystals of the heterobimetallic MCPs suggests that Cu on the trinuclear site of UMCM-150 was replaced by the other metal, whereas Cu in paddlewheel sites remains unchanged. N_2 sorption isotherms were measured for the mixed-metal UMCM-150 analogues, and it was confirmed that there is no structural collapse after the metal replacement.

Introduction

The recent explosion in the number of porous coordination polymers reported has been fueled primarily through a combination of new organic linker design and the realization of many possible modes from the connection of these units by metals and metal clusters.[1−9] Recently, we disclosed the utility of biphenyl-3,4′,5-tricarboxylic acid (H_3BHTC) in the production of a microporous coordination polymer (MCP) based on coordination to Cu^{II}.[10] One unprecedented feature of this material, dubbed University of Michigan Crystalline Material 150 (UMCM-150), is the presence of trinuclear copper clusters. The formation of a new secondary building unit (SBU) could be significant for novel MCP construction, and therefore testing the generality of this motif is desirable. Here we report studies on homometallic and heterobimetallic MCPs derived from this linker and find that structures based on UMCM-150 as well as those with an hourglass structure can be obtained depending on the metal identity.

In approaching the problem of constructing isostructural analogues of UMCM-150, screening different metal salts presents the most straightforward avenue albeit with a considerable risk of inducing new structure types. Therefore, a more minimally perturbative approach of metal substitution was also considered. In particular, the strategy that we recently employed to take advantage of two differing coordination environments to yield heterobimetallic MCPs was adopted.[1] UMCM-150 has both paddlewheel binding sites and trigonal-prismatic trinuclear clusters. The trinuclear motif is extremely rare for copper,[10−12] and therefore we reasoned that the direct replacement of copper in the trinuclear sites could be achieved by adding transition metals reported to form trinuclear clusters with carboxylic acids. Here we present heterobimetallic UMCM-150 analogues $Co_1Cu_2(BHTC)_2$ (**4**), $Fe_1Cu_2(BHTC)_2$ (**5**), and $Mn_1Cu_2(BHTC)_2$ (**6**) obtained by mixing Mn^{II}, Co^{II}, or Fe^{III} with Cu^{II} and H_3BHTC.

Experimental Section

General Information. H_3BHTC was prepared by the published procedure.[10] All solvents and metal complexes were used as received without further purification from Sigma-Aldrich

*To whom correspondence should be addressed. E-mail: matzger@umich.edu.

(1) Caskey, S. R.; Matzger, A. J. *Inorg. Chem.* **2008**, *47*, 7942.
(2) Ren, P.; Shi, W.; Cheng, P. *Cryst. Growth Des.* **2008**, *8*, 1097.
(3) Cheng, J. W.; Zhang, J.; Zheng, S. T.; Ma, E.; Yang, G. Y. *Inorg. Chem.* **2007**, *46*, 10534.
(4) Ouyang, Y.; Zhang, W.; Xu, N.; Xu, G. F.; Liao, D. Z.; Yan, S. P.; Cheng, P. *Inorg. Chem.* **2007**, *46*, 8454.
(5) Zhao, X. Q.; Zhao, B.; Ma, Y.; Shi, W.; Cheng, P.; Jiang, Z. H.; Liao, D. Z.; Yan, S. P. *Inorg. Chem.* **2007**, *46*, 5832.
(6) Luo, F.; Hu, D. X.; Xue, L.; Che, Y. X.; Zheng, J. M. *Cryst. Growth Des.* **2007**, *7*, 851.
(7) Zhai, B.; Yi, L.; Wang, H. S.; Zhao, B.; Cheng, P.; Liao, D. Z.; Yan, S. P. *Inorg. Chem.* **2006**, *45*, 8471.
(8) Rizzi, A. C.; Calvo, R.; Baggio, R.; Garland, M. T.; Pena, O.; Perec, M. *Inorg. Chem.* **2002**, *41*, 5609.
(9) Cheng, J. W.; Zhang, J.; Zheng, S. T.; Zhang, M. B.; Yang, G. Y. *Angew. Chem., Int. Ed.* **2006**, *45*, 73.
(10) Wong-Foy, A. G.; Lebel, O.; Matzger, A. J. *J. Am. Chem. Soc.* **2007**, *129*, 15740.
(11) Clerac, R.; Cotton, F. A.; Dunbar, K. R.; Hillard, E. A.; Petrukhina, M. A.; Smucker, B. W. C. R. *Acad. Sci. Paris, Chim/Chem.* **2001**, *4*, 315.
(12) Cage, B.; Cotton, F. A.; Dalal, N. S.; Hillard, E. A.; Rakvin, B.; Ramsey, C. M. *J. Am. Chem. Soc.* **2003**, *125*, 5270.

Published on Web 05/10/2010

and Fisher Scientific. For gas sorption experiments, N_2 (99.999%) and Ar (99.999%) were purchased from Cryogenic Gasses and used as received. An Autosorb-1C outfitted with the micropore option from Quantachrome Instruments (Boynton Beach, FL) was used to measure N_2 adsorption/desorption at 77 K and Ar adsorption/desorption at 87 K. The surface areas of all materials and a pore-size distribution of $Mg_3(BHTC)_2$ (**2**) were calculated with version 1.2 of the *ASWin* software package. The pressure range of $3.00 \times 10^{-3} < P/P_0 < 1.00 \times 10^{-1}$ was used for the measurement of the surface area. For the pore-size distribution of **2**, the range of P/P_0 was between 1.00×10^{-4} and 8×10^{-1} with Ar sorption at 87 K. Pore-size distributions were calculated using the nonlinear density functional theory (NLDFT) zeolite/silica equilibrium transition kernel for Ar adsorption based on a cylindrical pore model as implemented in version 1.2 of the *ASWin* software package. Powder X-ray diffraction (PXRD) patterns were obtained on a Rigaku R-Axis Spider diffractometer with samples mounted on Nylon loops and coated with mineral oil. Images were collected in transmission mode with χ set at 45°, φ rotating at 10°/min, and ω oscillating between 120° and 180° at 1°/min. The *AreaMax* (2.0) software package was used for integration of the resulting images with a step size of 0.1° in 2θ. The metal species in heterobimetallic UMCM-150 analogues were confirmed with energy-dispersive X-ray (EDX) spectroscopy using a Hitachi S-3200N scanning electron microscope. An Optima 2000 DV inductively coupled plasma optical emission spectrometer from Perkin-Elmer Instruments was used to quantify the relative amounts of metal species in the heterobimetallic UMCM-150 analogues. These ratios were used to derive the formulas presented in the Experimental Section. Ratios of less than the ideal stoichiometry likely correspond to UMCM-150 analogues with trinuclear metal clusters, where Cu is only partially substituted by the second metal. For clarity of the presentation, the formula units of the UMCM-150 analogues are presented below as a mixture of pure phases. Thermogravimetric analysis (TGA) data were obtained with a TA Q50 apparatus.

X-ray Structure Determination. X-ray diffraction data were collected with a Rigaku R-Axis Spider diffractometer. Crystals of **1**, **4**, and **5** were exchanged in CH_2Cl_2 and coated in paratone N oil. The colorless needle for **1** and the blue and green hexagonal plates for **4** and **5** were mounted on a MitiGen cryoloop and cooled under a N_2 gas stream at 253(2) K. Data were collected using the d*TREK package in the *CrystalClear* software suite (version 1.4, Rigaku 2007) to obtain overlapping φ and ω scans. Using the FS_PROCESS package in *CrystalClear*, the raw intensity data were then reduced to F^2 values with corrections for Lorentz and polarization effects. Decay of the crystal during data collection was negligible. An empirical absorption correction was applied, as implemented by FS_PROCESS. The structure was solved by direct methods and refined against all data using the *CrystalStructure* (version 3.8.2) software package in the trigonal space group $R\bar{3}$ (No. 148) and $Z = 9$ for **1**, the hexagonal space group $P63/mmc$ (No. 194) and $Z = 6$ for **4**, and $P63/mmc$ (No. 194) and $Z = 6$ for **5**.[13] Hydrogen atoms were placed at calculated positions (C−H = 0.95 Å) using a riding model with isotropic thermal parameters 1.2 times that of the attached carbon atom. Thermal parameters for all non-hydrogen atoms were refined anisotropically. Attempts to locate and model the highly disordered solvent molecules in the pores were unsuccessful. Therefore, the SQUEEZE routine of *PLATON*[14] was used to remove the diffraction contribution from guests to produce a set of solvent-free diffraction intensities.

(13) Sheldrick, G. M. *SHELXS '97 and SHELXL '97*; University of Gottingen: Gottingen, Germany, **1997**.

(14) Spek, A. L. *PLATON, A Multipurpose Crystallographic Tool*; Utrecht University: Utrecht, The Netherlands, **2005**.

Syntheses. Preparation of $Mn_3(BHTC)_2$ (1). H_3BHTC (0.20 g, 0.70 mmol) was dissolved in a mixture of *N*,*N*-dimethylformamide (DMF)/ethanol/H_2O (24 mL/6 mL/6 mL). $MnCl_2 \cdot 4H_2O$ (0.28 g, 1.4 mmol) was added and the homogeneous solution heated to 85 °C for 20 h. Colorless needle crystals were obtained. The yield was 27% based on H_3BHTC after drying under vacuum. Analysis for $(Mn_3C_{30}H_{14}O_{12})(C_3H_6NO)_2(H_2O)_4$ (fw = 947.0). Found (calcd): C, 46.19 (45.62); H, 3.55 (3.62); N, 2.90 (2.96).

Preparation of $Mg_3(BHTC)_2$ (2). H_3BHTC (0.025 g, 0.087 mmol) was dissolved in a DMF/ethanol mixture (6 mL/1.5 mL). To this solution was added 0.65 mL of 0.20 M $Mg(NO_3)_2 \cdot 6H_2O$ (0.033 g, 0.13 mmol), and the solution was heated to 85 °C for 2 days. Colorless needle crystals were obtained after 2 days. The yield was 33% based on H_3BHTC after drying under vacuum. Analysis for $(Mg_3C_{30}H_{14}O_{12})(C_3H_6NO)_2(H_2O)_{10}$ (fw = 962.2). Found (calcd): C, 44.29 (44.90); H, 4.97 (4.82); N, 2.97 (2.91).

Preparation of $Co_3(BHTC)_2$ (3). H_3BHTC (0.025 g, 0.087 mmol) was dissolved in a mixture of 6 mL of DMF and 1.5 mL of ethanol. To this solution was added 0.65 mL of 0.20 M $Co(NO_3)_2 \cdot 6H_2O$ (0.038 g, 0.13 mmol), and the solution was heated to 85 °C. Pink needle crystals were obtained after 3 days. The yield was 53% based on H_3BHTC after drying under vacuum. Analysis for $(Co_3C_{30}H_{14}O_{12})(C_3H_6NO)_{1.5}(H_2O)_8$ (fw = 995.0). Found (calcd): C, 41.61 (41.71); H, 3.95 (3.96).

Preparation of the UMCM-150 Analogue $Co_1Cu_2(BHTC)_2$ (4). H_3BHTC (0.025 g, 0.087 mmol) and 0.60 mL of 0.20 M $Co(NO_3)_2 \cdot 6H_2O$ (0.035 g, 0.12 mmol) were added to a solution of DMF/ethanol (6 mL/1.5 mL). To this mixture was added 0.35 mL of 0.20 M $Cu(NO_3)_2 \cdot 2.5H_2O$ (0.016 g, 0.070 mmol), followed by 0.25 mL of 0.40 M HCl. The solution was heated at 85 °C for 30 h to yield blue hexagonal plate crystals. The yield was 29% based on H_3BHTC after drying under vacuum. Analysis for $(C_{15}H_7O_6)_2Cu_2Co)_{0.75}((C_{15}H_7O_6)_2Cu_3)_{0.25}(H_2O)_6$ (fw = 859.9). Found (calcd): C, 41.56 (41.86); H, 3.02 (3.05). The contents of Cu and Co were analyzed by inductively coupled plasma optical emission spectrometry (ICP-OES): Co, 5.17 (5.14); Cu, 16.37 (16.46).

Preparation of the UMCM-150 Analogue $Fe_1Cu_2(BHTC)_2$ (5). H_3BHTC (0.0050 g, 0.017 mmol) and 0.07 mL of 0.20 M $Fe(NO_3)_3 \cdot 9H_2O$ (0.0056 g, 0.014 mmol) were added to DMF/dioxane (1.2 mL/0.3 mL). To this mixture was added 0.20 mL of 0.20 M $Cu(NO_3)_2 \cdot 2.5H_2O$ (0.0093 g, 0.040 mmol), followed by 0.25 mL of acetic acid. The solution was heated for 1 day at 85 °C to yield green hexagonal plate crystals. The yield was 55% based on H_3BHTC after drying under vacuum. Analysis for $((C_{15}H_7O_6)_2Cu_2Fe_1(\mu_3\text{-}O)_{0.33}(OH)_{0.33})_{0.85}((C_{15}H_7O_6)_2Cu_3)_{0.15}(H_2O)_7$ (fw = 893.3). Found (calcd): C, 39.42 (40.30); H, 3.23 (3.19). The contents of Cu and Fe were analyzed by ICP-OES: Fe, 5.33 (5.32); Cu, 15.42 (15.14).

Preparation of the UMCM-150 Analogue $Mn_1Cu_2(BHTC)_2$ (6). $MnCl_2 \cdot 4H_2O$ (0.16 g, 0.81 mmol) and H_3BHTC (0.050 g, 0.17 mmol) were dissolved in a DMF/ethanol/H_2O (10 mL/2.5 mL/1.5 mL) mixture. The solution was sonicated for 45 min, followed by the slow addition of 0.70 mL of 0.20 M $Cu(NO_3)_2 \cdot 2.5H_2O$ (0.032 g, 0.14 mmol). The solution was heated at 75 °C for 20 h. Pale-green hexagonal plate crystals were obtained. The yield was 10% based on H_3BHTC after drying under vacuum. Analysis for $((C_{15}H_7O_6)_2Cu_2Mn)_{0.76}((C_{15}H_7O_6)_2Cu_3)_{0.24}(H_2O)_7$ (fw = 874.8). Found (calcd): C, 42.46 (41.15); H, 3.23 (3.22). The contents of Cu and Mn were analyzed by ICP-OES: Mn, 4.79 (4.77); Cu, 16.18 (16.11).

Results and Discussion

The coordination of Cu^{II} to carboxylates in coordination polymers is dominated by the paddlewheel motif. It was therefore remarkable when, for the first time, a trinuclear copper cluster coordinating to six carboxylates was

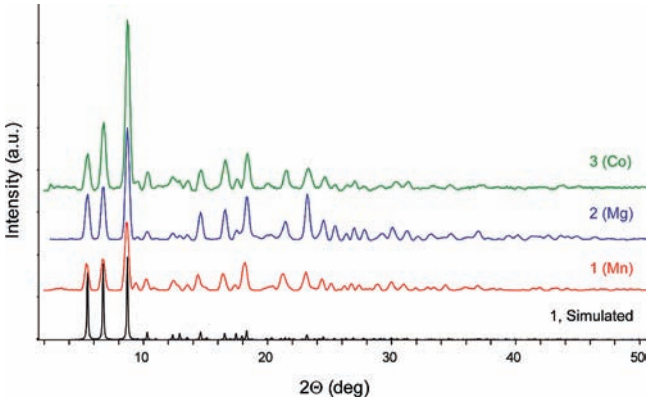

Figure 1. PXRD data for **1**−**3** compared to the simulated pattern for **1**.

discovered.[10] The linker that gave rise to this unique geometry is H_3BHTC, and this linker is itself the first example of the employment of a reduced-symmetry all-carboxylate linker in which the coordinating groups do not behave as if they are equivalent by symmetry. The compound arising from BHTC and Cu, UMCM-150, is therefore of interest for containing a novel SBU that, if generalizable, might lead to new coordination polymer structure classes with corresponding novel properties. In the search for additional examples of trinuclear clusters, only a few metal ions, such as Co^{II}, Fe^{III}, and Mn^{II}, are known to form this motif in combination with carboxylic acids for MCPs.[15−18] In order to probe the possibility that these metals would generate the trinuclear cluster while retaining the UMCM-150 structure, studies of the reaction of these metal ions with H_3BHTC were undertaken. In addition, the reaction of H_3BHTC and Mg^{II}, a light metal with no structural evidence of forming homometallic trinuclear clusters,[19] was studied for structural comparison with previous MCPs. There is increasing activity in incorporating light metals into MCPs, and recently very promising results have been reported for Be;[20,21] however, concerns regarding Be toxicity limit our current investigations to Mg.

Solvothermal reactions at 85 °C of H_3BHTC and Mn^{II}, Mg^{II}, and Co^{II} metal salts yielded the MCPs **1**−**3** respectively. PXRD confirmed that these materials are isostructural (Figure 1) and, furthermore, do not adopt the structure of UMCM-150. Indeed, single-crystal X-ray analysis indicates that each structure consists of six BHTC ligands coordinated to three octahedral metal centers arranged linearly. This particular trinuclear metal cluster has been termed the hourglass SBU,[22] and, in fact, the Mg member of this series

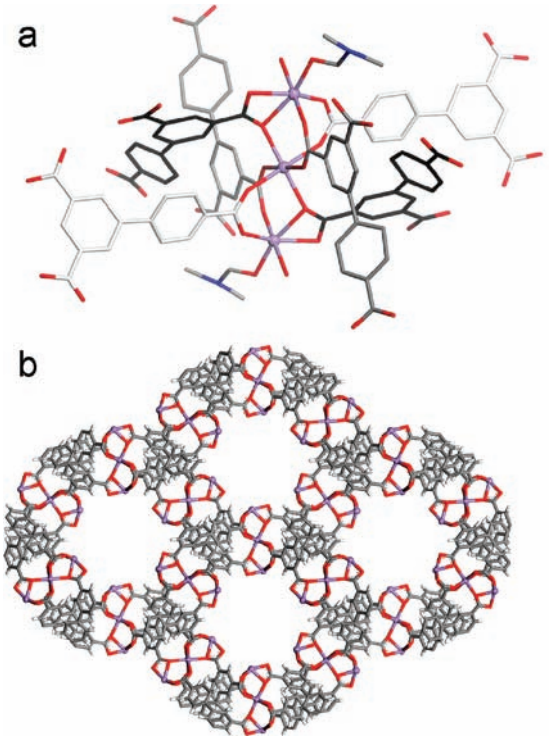

Figure 2. (a) Six BHTC linkers coordinate to three Mn^{II} ions, forming an hourglass shape in **1**. Hydrogen atoms have been removed for clarity. (b) Channels running along the *c* axis in **1**. Coordinating groups have been removed for an unobstructed view.

was recently disclosed.[23] The central Mn^{2+} is octahedrally coordinated to six carboxylates, four isophthalate groups, and two carboxyphenyl carboxylate groups from the BHTC linker. Terminal metal ions are bound by three carboxylate groups: two bridging carboxylates (carboxyphenyl and isophthalate) and a chelating isophthalate−carboxylate (Figure 2a). Additionally, one DMF and one H_2O molecule coordinate to each axial position and can be removed, generating coordinatively unsaturated metal sites. The structure of the Mn compound consists of one-dimensional hexagonal channels with an atom-to-atom diameter of 11.5 Å (Figure 2b), and X-ray crystallographic details of the Mn analogue are listed in Table 1. These materials display good surface areas (vide infra) and a cylindrical pore structure reminiscent of the well-studied M/DOBDC series.[24−27]

Although hourglass SBUs are formed in homometallic Mn^{II} and Co^{II} MCP structures with the BHTC linker, they have also been known to adopt the trigonal-prismatic $M_3(CO_2R)_6$ trinuclear cluster, with other ligands.[15−17,28] Fe^{III} can also form this cluster geometry,[18] rendering these metals appropriate candidates for substitution into the UMCM-150 structure to form heterobimetallic analogues. In each of these cases, the reaction conditions were carefully chosen to minimize the formation of homometallic hourglass-based

(15) Vrubel, H.; Hasegawa, T.; Oliveira, E. d.; Nunes, F. S. *Inorg. Chem. Commun.* **2006**, *9*, 208.
(16) Sudik, A. C.; Millward, A. R.; Ockwig, N. W.; Cote, A. P.; Kim, J.; Yaghi, O. M. *J. Am. Chem. Soc.* **2005**, *127*, 7110.
(17) Moriya, M.; Ito, M.; Sakamoto, W.; Yogo, T. *Cryst. Growth Des.* **2009**, *9*, 1889.
(18) Yoon, J. H.; Choi, S. B.; Oh, Y. J.; Seo, M. J.; Jhon, Y. H.; Lee, T.-B.; Kim, D.; Choi, S. H.; Kim, J. *Catal. Today* **2007**, *120*, 324.
(19) Both Mg/Cr and Mg/Fe trinuclear clusters have been reported: Turta, C.; Shova, S.; Prodius, D.; Mereacre, V.; Gdaniec, M.; Simonov, Y.; Lipkowski, J. *Inorg. Chim. Acta* **2004**, *357*, 4396–4404.
(20) Porter, W. W.; Wong-Foy, A.; Dailly, A.; Matzger, A. J. *J. Mater. Chem.* **2009**, *19*, 6489.
(21) Sumida, K.; Hill, M. R.; Horike, S.; Dailly, A.; Long, J. R. *J. Am. Chem. Soc.* **2009**, *131*, 15120.
(22) Catterick, J.; Hursthouse, M. B.; New, D. B.; Thornton, P. *Chem. Commun.* **1974**, 843.
(23) Guo, Z.; Li, G.; Zhou, L.; Su, S.; Lei, Y.; Dang, S.; Zhang, H. *Inorg. Chem.* **2009**, *48*, 8069.
(24) Caskey, S. R.; Wong-Foy, A. G.; Matzger, A. J. *J. Am. Chem. Soc.* **2008**, *130*, 10870.
(25) Rosi, N. L.; Kim, J.; Eddaoudi, M.; Chen, B. L.; O'Keeffe, M.; Yaghi, O. M. *J. Am. Chem. Soc.* **2005**, *127*, 1504.
(26) Dietzel, P. D. C.; Johnsen, R. E.; Blom, R.; Fjellvag, H. *Chem.—Eur. J.* **2008**, *14*, 2389.
(27) Dietzel, P. D. C.; Morita, Y.; Blom, R.; Fjellvag, H. *Angew. Chem., Int. Ed.* **2005**, *44*, 6354.
(28) Ma, S.; Simmons, J. M.; Yuan, D.; Li, J.-R.; Weng, W.; Liu, D.-J.; Zhou, H.-C. *Chem. Commun.* **2009**, *27*, 4049.

Table 1. Crystallographic Data for **1**, **4**, and **5**

	1	**4**	**5**
empirical formula	$C_{36}H_{28}Mn_3N_2O_{16}$	$C_{30}H_{14}CoCu_2O_{15}$	$C_{30}H_{14}Cu_2Fe_1O_{15.3}$
fw	909.42	800.42	802.16
temperature, K	253(2)	253(2)	253(2)
wavelength	1.541 80	1.541 80	1.541 80
cryst syst	trigonal	hexagonal	hexagonal
space group	$R\bar{3}$ (No. 148)	$P63/mmc$ (No. 194)	$P63/mmc$ (No. 194)
unit cell dimensions			
a, Å	32.1587(12)	18.431(14)	18.452(3)
b, Å	32.1587(12)	18.431(14)	18.452(3)
c, Å	14.8229(6)	40.52(4)	40.925(11)
α, deg	90	90	90
β, deg	90	90	90
γ, deg	120	120	120
volume, Å^3	13275.8(9)	11922(17)	12067(5)
Z	9	6	6
density (calcd), g/cm^3	1.024	0.656	0.663
abs coeff, mm^{-1}	5.577	2.481	2.302
F(000)	4149	2346	2404
cryst size, mm^3	0.32 × 0.08 × 0.03	0.13 × 0.13 × 0.03	0.12 × 0.11 × 0.03
reflns collected/unique	18 108/5128	27 472/2389	24 287/2414
R(int)	0.1082	0.1109	0.0714
data completeness, % (2θ)	98.5 (66.59)	99.7 (66.59)	100.0 (50.50)
abs corrn	empirical from equivalents	empirical from equivalents	empirical from equivalents
max and min transmn	0.851 and 0.268	0.929 and 0.739	0.924 and 0.725
refinement method	full-matrix least squares on F^2	full-matrix least squares on F^2	full-matrix least squares on F^2
restraints/param	0/260	0/120	0/144
GOF on F^2	1.082	1.018	1.016
final R indices [$I > 2\sigma(I)$][a,b]	R1 = 0.1322	R1 = 0.0928	R1 = 0.0418
	wR2 = 0.3575	wR2 = 0.2710	wR2 = 0.1094
R indices (all data)[a,b]	R1 = 0.2086	R1 = 0.1346	R1 = 0.0509
	wR2 = 0.4133	wR2 = 0.2971	wR2 = 0.1141

[a] $wR2 = |\sum w(|F_o|^2 - |F_c|^2)|/\sum|w(F_o)^2|^{1/2}$, $w = 1/[\sigma^2(F_o^2) + (mP)^2 + nP]$ and $P = [\max(F_o^2,0) + 2F_c^2)]/3$ (m and n are constants); $\sigma = [\sum[w(F_o^2 - F_c^2)^2]/(n-p)]^{1/2}$. [b] $R1 = \sum||F_o| - |F_c||/\sum|F_o|$.

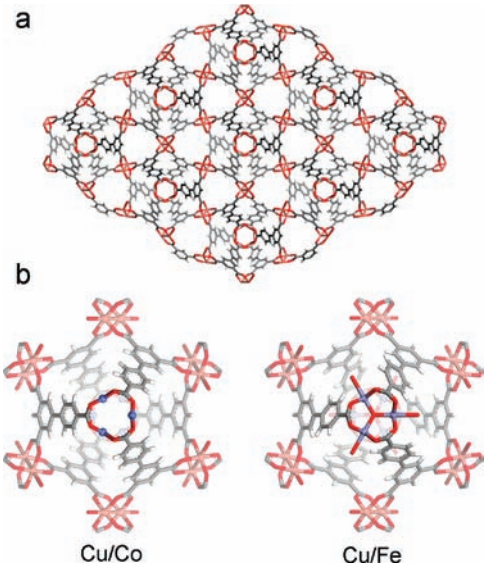

Figure 3. (a) Structure of UMCM-150 adapted by heterobimetallic analogues (coordinating H_2O molecules have been removed for clarity). (b) View of the paddlewheel and trinuclear clusters in **4** (Cu/Co) and **5** (Cu/Fe). The structure of **5** features an μ_3-O in the center of the trinuclear cluster and one hydroxide and two H_2O molecules bound to the Fe^{III} ions. Color scheme: bronze sphere, Cu; gray, C; red, O; blue sphere, Co; cyan sphere, Fe.

materials and favor pure UMCM-150 phases. Mixed-metal solutions were subjected to solvothermal conditions to yield MCPs **4**−**6** consisting of Co/Cu, Fe/Cu, and Mn/Cu metal clusters. Scanning electron microscopy (SEM) with EDX confirmed the existence of two types of metal species in **4**−**6**

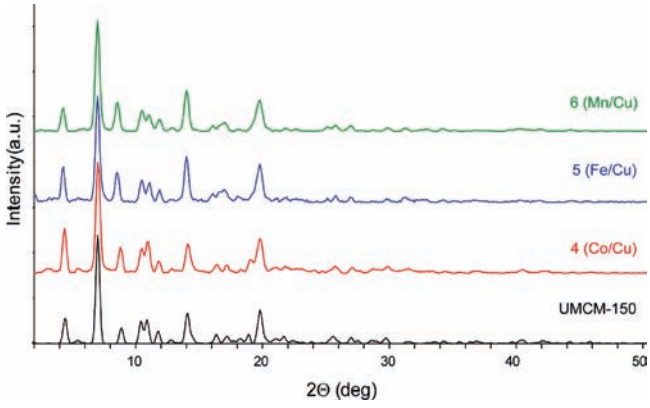

Figure 4. PXRD data of **4**−**6** compared to the pattern for UMCM-150.

(Figure S1a−c in the Supporting Information). Single-crystal X-ray diffraction indicates that Co and Fe ions occupy the trinuclear metal cluster positions (Figure 3). Although each MCP is isostructural with UMCM-150 (Figure 4), the Fe/Cu heterobimetallic analogue **5** has a modified trinuclear cluster to accommodate the Fe^{III} oxidation state. This cluster has a μ_3-O^{2-} in the center of the trinuclear Fe cluster (Figure 3). Each Fe^{3+} is six-coordinate, with four carboxylates binding to each Fe in a square-planar geometry. One axial position of each Fe is occupied by the μ_3-O oxygen at the center of the cluster, while the position trans hosts a solvent molecule. Overall, each $Fe_3(\mu_3\text{-}O)(CO_2R)_6$ cluster has three bound solvent molecules with two occupied by H_2O and the third by a hydroxide group in order to compensate for the extra charge of the cluster.

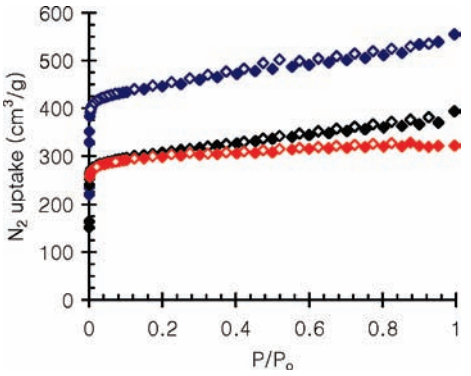

Figure 5. N_2 isotherms of **1**−**3** at 77 K (solid diamond, adsorption; open diamond, desorption; dark blue, **2**; gray, **3**; red, **1**).

Bulk analysis of UMCM-150 analogues **4**−**6** was undertaken using ICP-OES to quantify the metal content distribution in the heterobimetallic systems. Assuming complete substitution of the trinuclear cluster with Co, Fe, and Mn, a molar ratio of 1:2 is expected between these metals and Cu. For **4**, a ratio of 1:3.05 is found, revealing incomplete substitution of the trinuclear sites. With this same approach, the molar ratio of Fe/Cu was found to be 1:2.52 and that of Mn/Cu 1:2.88. Attempts to increase the incorporation of Co, Fe, or Mn by employing higher concentrations led to new phase formation and/or a lowering of the yield of the UMCM-150 analogues. Nonetheless, successful structural refinement of **4** and **5**, using a 1:2 ratio of Co/Fe to Cu suggests that the stoichiometries are reasonable, and this is supported by the well-behaved thermal parameters for metals in both sites.

N_2 Sorption Isotherms and Pore-Size Distributions. The surface areas of the monometallic MCPs with hourglass SBUs, **1**−**3**, were measured through N_2 sorption isotherms to verify their permanent porosity. Samples were prepared by soaking crystals in DMF for 1 day, followed by immersion and exchange in CH_2Cl_2 three times over the course of 3 days. Compound **2** was heated for 38 h at 110 °C for activation, whereas **1** and **3** were heated for 28 h at 100 °C. Structure **2** has the highest N_2 uptake, providing a Brunauer−Emmer−Teller (BET) surface area of 1690 m^2/g (1830 m^2/g, Langmuir; Figures 5 and S2a,b in the Supporting Information).[29] MCPs **1** and **3** have BET surface areas of 1175 and 1190 m^2/g (1270 and 1300 m^2/g, Langmuir), respectively. In this series, the highest value for the coordination polymer derived from Mg is consistent with the notion that lightweight metals improve the surface area by reducing the weight of the framework.[24,30] Only a slight difference in the surface area is observed for Co and Mn because the metals have similar molecular weights. A pore-size distribution for **2** using Ar sorption at 87 K shows a narrow pore size of 6−10 Å, which is consistent with the crystal structure and is highly desirable for adsorptive applications (Figures S3 and S4 in the Supporting Information).

(29) This value is substantially higher that that reported in reference 23 suggesting a superior activation procedure or improved phase purity.

(30) Schnobrich, J. K.; Koh, K.; Sura, K. N.; Matzger, A. J. *Langmuir* **2010**, *26*, 5808.

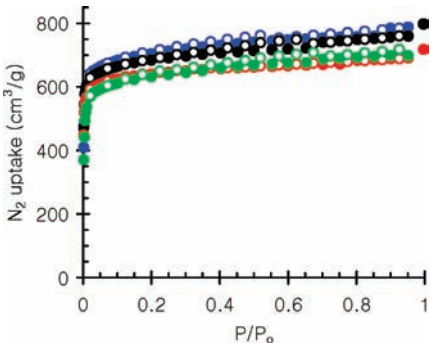

Figure 6. N_2 uptake of heterobimetallic UMCM-150 analogues at 77 K (solid circle, adsorption; open circle, desorption; blue, UMCM-150; green, **4**; black, **5**; red, **6**).

Activation of the heterobimetallic UMCM-150 analogues **4**−**6** was achieved by immersion in DMF, followed by exchange into CH_2Cl_2 three times over the course of 3 days. The solvent-exchanged crystals were then heated for 20 h at 100 °C. The N_2 sorption isotherm of UMCM-150 indicates a BET surface area of 2715 m^2/g (3011 m^2/g, Langmuir). Substitution of Co, Fe, and Mn in the trinuclear metal cluster positions, generating structures **4**−**6**, produced surface areas of 2441, 2660, and 2490 m^2/g (2686, 2920, and 2750 m^2/g, Langmuir), respectively (Figure 6). The similarity between the surface areas of these heterobimetallic UMCM-150 analogues indicates that selective metal substitution is a suitable method for creating a diverse set of structurally related MCPs without drastically altering their N_2 sorption properties.

Conclusion

The results presented here show that BHTC is a versatile linker that can accommodate different high-surface-area phases depending on the identity of the metal. One-dimensional hexagonal channel structures are formed when the metal prefers to form the hourglass SBU, as demonstrated for MCPs **1**−**3**. On the other hand, in the heterobimetallic systems, the presumably faster formation of the Cu^{II} paddlewheel SBU drives the formation of the UMCM-150 structure, while the trigonal-prismatic SBU is generated with the second transition metal. This is demonstrated for Co^{II}, which in the absence of Cu forms **3**, whereas in the presence of Cu, **4** is formed. Applications of these MCPs in gas separation and catalysis are underway.

Acknowledgment. We acknowledge support of this work through Grant 454 of the 21st Century Jobs Trust Fund received through the SEIC Board from the State of Michigan. We also acknowledge the National Science Foundation for providing funding for the Hitachi S-3200N scanning electron microscope (Award No. EAR-96-28196).

Supporting Information Available: Complete X-ray crystallographic data for **1**, **4**, and **5** in CIF format, EDX data from SEM (Figure S1a−c), typical BET and Langmuir fits for the surface-area measurement of **2** with N_2 sorption isotherm data (Figure S2a, b), pore-size distribution and NLDFT fit for **2** (Figures S3 and S4), and TGA for **1**−**6** (Figure S5a,b). This material is available free of charge via the Internet at http://pubs.acs.org.